Heliyon 10 (2024) e27124

Contents lists available at ScienceDirect

Heliyon

journal homepage: www.cell.com/heliyon

Research article

Modification of structural, morphological, and dielectric properties of barium calcium titanate ceramics with yttrium addition

Hasnat Jahan Sumona, Abdullah Al Mahmood *, M. Bodiul Islam, Jahid Hasan Kasem, M.S. Rahman

Department of Glass & Ceramic Engineering, Rajshahi University of Engineering & Technology, Rajshahi, 6204, Bangladesh

ARTICLE INFO

Keywords:
Yttrium
Barium calcium titanate ceramics
Sintering
Grain size
Capacitor

ABSTRACT

Barium calcium titanate (BCT) ceramics with varying yttrium doping concentrations were fabricated using the solid-state compaction process to explore the attributes of dopants. $(Ba_{0.75}Ca_{0.25})\ TiO_3$ and $(Ba_{0.75}Ca_{0.25})\ (Y_yTi_{(1-y)})\ O_3$ where, y = 0.00, 0.10, 0.15, and 0.20 ceramics were synthesized by pressing isostatically in pellet press apparatus, then sintered at 1250 °C with consequent cooling in furnace ambient. The structural, morphological, and dielectric properties were characterized using X-ray diffraction (XRD), scanning electron microscopy (SEM), and impedance spectroscopy interpretations, respectively. The XRD analysis revealed that the cubic BCT lattice was transformed into a tetragonal structure with Yttrium doping. Scanning electron microscopy (SEM) disclosed that yttrium doping countered the liquid phase formation of BCT as well as influenced grain development and microstructure, leading to the formation of distinct grain boundaries and improved densification. The average grain size (18–29 nm) of the Y-BCT increases as the doping level rises. At 60 Hz, it was reported that the dielectric constant obtained a maximum value of 70000 with a resistivity of 5×10^8 Ω-cm for y = 0.15. The manifestation of the secondary phase confirmed from XRD, allocating an easy path for oxygen migration, might be responsible for the rise in oxygen vacancy, higher leakage current, and dielectric loss for y = 0.01. Co-doping of calcium and yttrium in BCT ceramics has modified the basic structure and ameliorated composites' structural stability and dielectric characteristics. The optimized sample, upon demonstrating outstanding efficiency, ought to be employed for specific uses such as energy storage devices and capacitors.

1. Introduction

A greater variety of electronic devices need to be multifunctional and miniature due to the rapid advancement of the integrated circuit industry. Traditional $BaTiO_3$ ceramics, which have excellent ferroelectric properties, are used in a variety of electronic devices,

Abbreviations: BT, Barium titanate; CT, Calcium titanate; BCT, Barium calcium titanate; BCYT, Barium yttrium calcium titanate; Y- BCT, Barium-yttrium calcium titanate; β, Line widening at half the maximum intensity; σ, Electrical conductivity; δ, Dislocation density; λ, Wavelength; ε, Dielectric constant; τ, Crystallite size; t, Tolerance factor; τ′, Relaxation time; ϵ, Strain; Tanδ, Dielectric Loss; T, temperature.

* Corresponding author.
E-mail address: abdullah@gce.ruet.ac.bd (A. Al Mahmood).

https://doi.org/10.1016/j.heliyon.2024.e27124
Received 16 October 2023; Received in revised form 3 February 2024; Accepted 23 February 2024
Available online 27 February 2024

Fig. 1. Solid State Synthesis diagram of prepares sample.

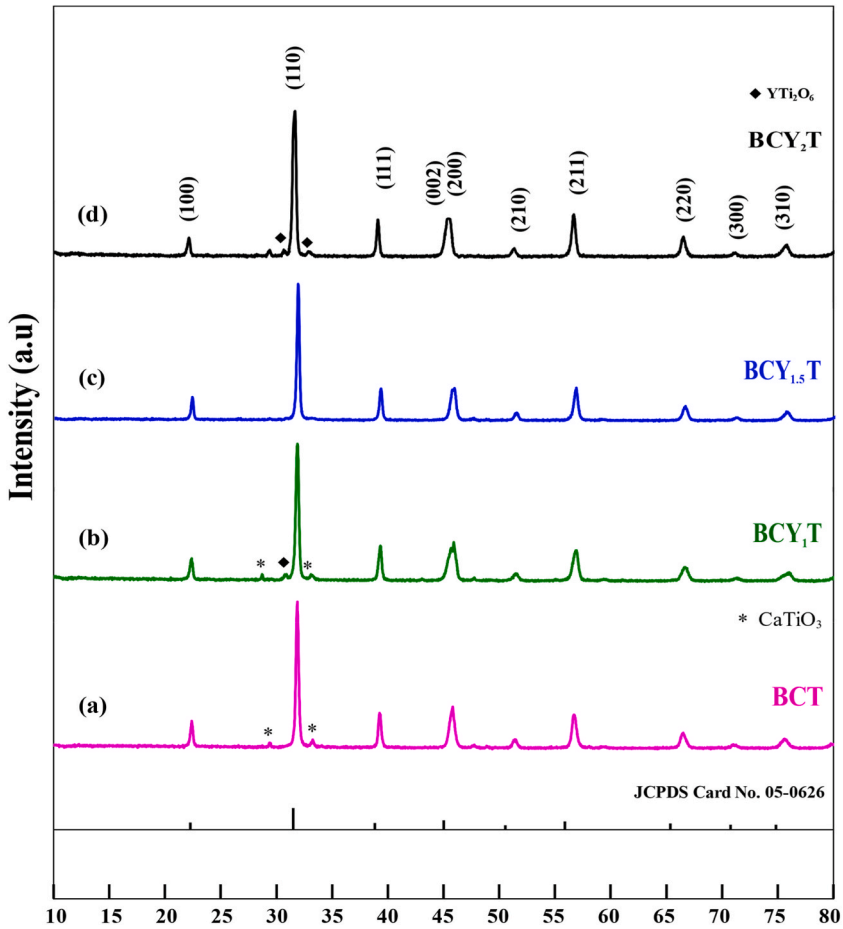

Fig. 2. XRD patterns of (a) BCT, (b) BCY_1T, (c) $BCY_{1.5}T$ and (d) BCY_2T ceramics.

such as multilayer ceramic capacitors [1]. To ensure the consistent operation of incredibly effective electronic circuits while taking variances in temperature into account, capacitors must develop novel compounds with high dielectric permittivity, small permittivity variability, and minimal dielectric loss across an extensive variety of temperatures [2]. The chemistry and geometry of ceramics profoundly influence the dielectric characteristics of capacitors. Controlling chemistry and geometry has thus emerged as a key strategy for enhancing the characteristics of $BaTiO_3$. Through the use of dopants, solid solutions, and fabrication techniques, numerous kinds of perovskite lead-free dielectrics have recently been used to modify the chemical structure or topology of ceramics [3].

Recent research has concentrated on lead-free and environmentally acceptable $BaTiO_3$-based dielectric compounds because of their substantial dielectric constant and polarization. Several lead-free piezoelectric ceramics, including potassium-sodium niobate (KNN), bismuth-potassium titanate (BKT), and bismuth-sodium titanate (BNT), have been explored over the past 20 years [4]. Nevertheless, these substances possess numerous adverse effects, including a minimal piezoelectric constant (d_{33}) and high conductivity, leading to current leakage. Due to the aforementioned difficulties with alkali-based systems, modified lead-free piezoelectric devices made of

Table 1
Structural parameters of BCT, BC_1YT, $BCY_{1.5}T$ and BCY_2T ceramics.

Composition	Lattice Parameter (a = b)Å	Lattice Parameter (c) Å	$\frac{c}{a}$	Cell volume Å^3	R Factor %	GoF	χ2
(BCT)	3.9739	3.9739	1	62.75	Rp = 8.40 Rwp = 10.7 Rexp = 4.77	1.9	3.58
(BCY_1T)	3.9806	3.9994	1.00472	63.37	Rp = 5.42 Rwp = 7.02 Rexp = 4.7	1.5	2.19
($BCY_{1.5}T$)	3.9805	3.9994	1.00474	63.36	Rp = 6.70 Rwp = 7.31 Rexp = 4.99	1.7	3.07
(BCY_2T)	3. 8749	4.0037	1.00421	63.25	Rp = 5.54 Rwp = 7.31 Rexp = 4.77	1.5	2.35

Table 2
Tolerance factor (t), strain (ϵ), dislocation density (δ) of BCT, BCY_1T, $BCY_{1.5}T$ and BCY_2T ceramics.

Composition	Ionic Radii Nm		Tolerance Factor, t	Strain, ϵ Nm	Dislocation density,δ Nm^{-2}
	A-site	B-site			
(BCT)	0.1286	0.0680	1.01101	4.13	2.30
(BCY_1T)	0.1286	0.0683	1.00886	4.44	2.46
($BCY_{1.5}T$)	0.1286	0.0685	1.0074	6.52	7.42
(BCY_2T)	0.1286	0.0687	1.0063	8.04	10.74

Table 3
Structural properties of the prepared of BCT, BCY_1T, $BCY_{1.5}T$ and BCY_2T ceramics.

Composition	Crystallite size, τ (nm)	Density, ρ_{exp} (gcm^{-3})	Average Grain Size, (nm)	Percent Porosity %	Crystallinity (%)	Xrd Density, ρ_{exp} (gcm^{-3})
(BCT)	16.58	2.86	18.48	53	62	6.111
(BCY_1T)	20.12	3.29	24.53	47	67	6.267
($BCY_{1.5}T$)	21.12	4.44	26.57	27	71	6.513
(BCY_2T)	22.41	4.25	29.28	35	69	6.573

barium titanate ($BaTiO_3$) are recommended [5]. The impact of Calcium doping on the dielectric characteristics of $BaTiO_3$ in the solid solution of $Ba_{1-x}Ca_xTiO_3$ (BCT) has received a lot of attention [6,7]. In fact, calcium inhibits reduction in $BaTiO_3$ and lowers the chance of the undesirable hexagonal phase forming [8].

CaO effectively limits the formation of the grains, enhances the electromechanical characteristics, and expands the temperature range where the tetragonal state is stable [9,10]. Another major depressor is $CaTiO_3$ (CT), which lowers the BT system's dielectric loss. $Ba_{1-x}Ca_xTiO_3$ (BCT) has been found to exist in a tetragonal phase for Ca^{2+} exchange (as a result of limited solubility, upwards of x = 0.25), that only marginally alters Curie Temperature (T_C) but significantly affects dielectric characteristics. Ca^{2+} propensity to take over simultaneously A-site and B-site ions may offer several useful properties. Consequently, BCT is recognized as one of the potential alternatives for the risky PZT system electro-optic modulator [11,12]. Devries and Roy [13] investigated the phase relationships in the $BaTiO_3$–$CaTiO_3$ system. They conducted a phase analysis using a $BaTiO_3$ solution at 1400 °C. The effects of calcium ion replacement on the ferroelectric structural transitions and dielectric properties of $BaTiO_3$ have been studied. A uniform solid is created by $CaTiO_3$ at up to 18 mol% [13]. While Mcquarrie and Behnke [14] reported that Ca-doped $BaTiO_3$ indicated a lowering of the Curie point, Berlincourte and Kulesar discovered that Ca^{2+} replacement in $BaTiO_3$ only generated minor alterations in the Curie point. The first to mention the potential presence of Ca^{2+} in both the Ba^{2+} and Ti^{4+} locations was Zhuang et al. [15] Following that, other writers executed to determine the site occupancy of Ca^{2+} in $BaTiO_3$ produced by various approaches to processing. Yet, modifications to the unit cell dimension, persistent tardiness, adjustments in the crystal system, or putative topological modifications do not directly indicate cation replacements and arranging in (Ba, Ca, and Ti) O_3 single crystals. To avoid suggesting a prior agreement on the placement of Ca^{2+} ions in the $BaTiO_3$ matrix, this formula was utilized [16].

Doping ceramics made of barium titanate with calcium has several drawbacks, including i) Calcium doping can make barium titanate ceramics' Curie temperature lower. ii) Whereas doping can improve some characteristics of barium titanate ceramics, it can also reduce some ferroelectric characteristics, including remanent polarization and coercive field. iii) Doping with calcium can change the crystal structure of the material or introduce new phases. These affect materials stability and mechanical properties. To minimize the negative aspects of doping with calcium several researchers tried mixing a variety of dopants with barium calcium titanate. For example, Sol-gel technology has been effectively employed to manufacture $Ba_{0.85}Ca_{0.15}Zr_{0.1}Ti_{0.9}O_3$ (BCZT) ceramics [17,18,19].

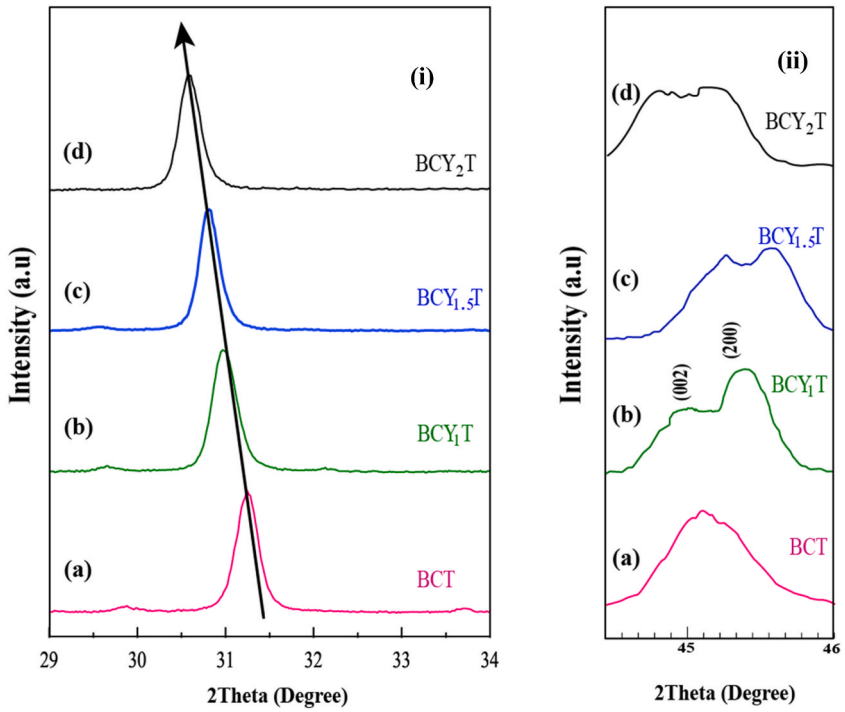

Fig. 3. **(a)** The peak shift pattern can be seen in the magnified section of the (110) peak in the region of 30°–32° on the spectrum of XRD of (a) BCT, (b) BCY_1T, (c) $BCY_{1.5}T$ and (d) BCY_2T ceramics and **(b)** structure enhanced between 44.5° and 46°.

Numerous studies have been conducted on the implications of rare earth dopants on the dielectric characteristics of barium titanate [20,21]. In barium titanate ceramics, yttrium doping has several benefits and can considerably enhance the material's characteristics for a variety of applications [22]. The following are some of the main benefits of yttrium doping: The dielectric features of yttrium-doped barium titanate ceramics are improved, including the dielectric constant and dielectric loss. These qualities are beneficial in capacitors and other electronic components, which call for materials with superior dielectric properties [23,24]. The mechanical hardness and toughness of ceramics made of barium titanate can be increased by yttrium doping. Barium titanate ceramics can receive controlled levels of yttrium doping to increase their electrical conductivity [25]. When both ionic and electronic conductivity are necessary, like in electrochemical sensors and solid oxide fuel cells, this characteristic is helpful [26]. Barium titanate ceramics can have their crystal structure stabilized by yttrium doping, which also prevents undesirable phases from forming [15]. As a result, phase transition resistance and material stability are improved. It's crucial to remember that the precise composition, concentration, and processing parameters determine how well yttrium doping mitigates the drawbacks of calcium doping [27,28]. To obtain the desired performance for their specific application, material scientists and engineers need to carefully adjust the dopant concentrations and processing parameters. The practice of co-doping with rare earth elements are successfully obtained. Doped with hafnium (H_f), Ba [$Zr_{0.2}Ti_{0.8}$] O_3 Ceramics made of (BZT) were created using the traditional solid-state reaction process [29].

In the present work, the combining effects of Calcium and Yttrium in barium titanate ceramics has been demonstrated. Secondary phase calcium titanate has developed, which has been found in the literature. The dielectric characteristics and material stability were deteriorated by the secondary phase [30]. Moreover, rare earth doping is becoming more and more common these days. For instance, yttrium is frequently used in barium titanate as one of the dopants. Yttrium can enhance material stability and stop unwanted phase development. In barium titanate, yttrium doping might lessen the negative effects of calcium doping. In the ABO_3 perovskite structure, ions are found to occupy both the A and B sites. This study looks at how the physical properties of doped BCT ceramics change, specifically how the presence of trivalent rare earth (RE) ions at the B-site affects these properties. The findings presented in this study enhance our comprehension of the physical characteristics shown by perovskite materials doped with rare earth elements. Using the solid-state reaction approach, structural, morphological, and dielectric research have also been explored. The purpose of this work is to evaluate the effects of co-doping barium titanate with calcium and yttrium in varying concentrations. The results of this work pave the way for future investigations and the creation of special functional materials with specific qualities for a range of technological applications.

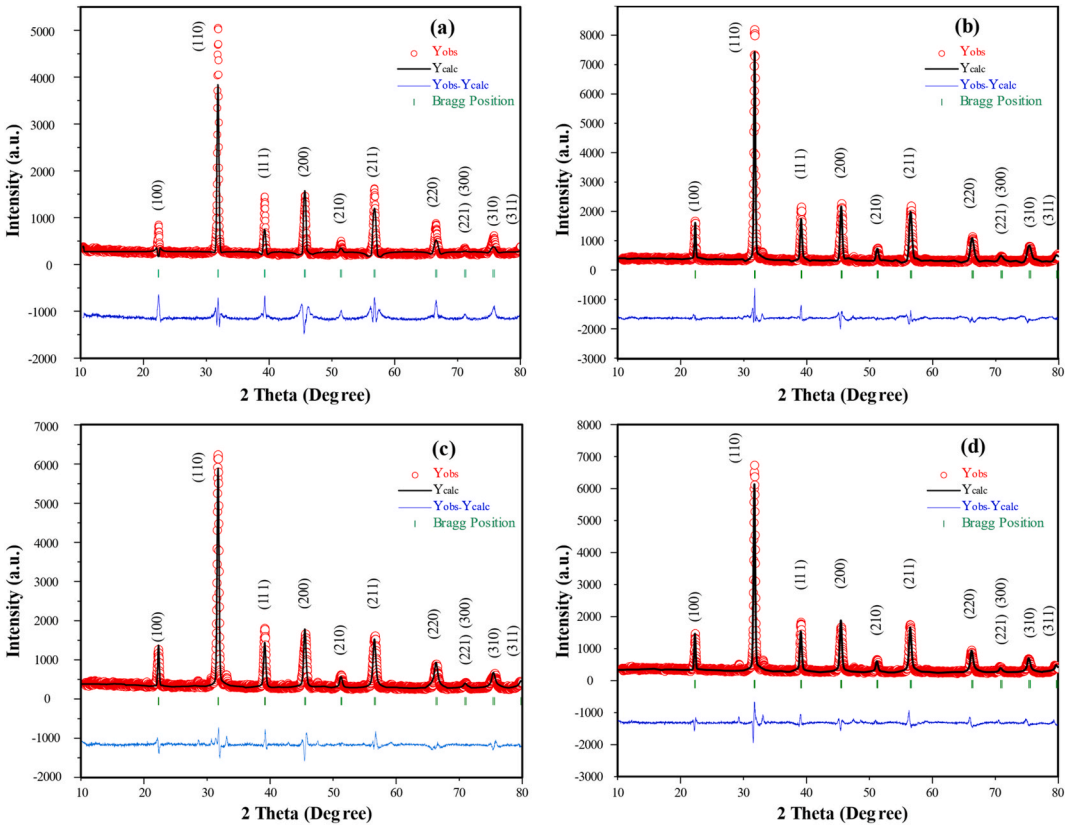

Fig. 4. Rietveld analysis of (a) BCT, (b) BCY_1T, (c) $BCY_{1.5}T$ and (d) BCY_2T ceramics.

2. Materials and methods

2.1. Materials

A standard solid-state sintering technique was implemented for fabricating $(Ba_{0.75}Ca_{0.25})$ $(Y_yTi_{(1-y)})O_3$ (y = 0.0, 0.10, 0.15, and 0.20) ceramic. The abbreviations for these ceramics are BCT, BCYT, $BCY_{1.5}T$ and BCY_2T respectively. Reagents needed for the investigation were $BaCO_3$ (Merck Specialities Pvt. Ltd, 99.95% Purity), $CaCO_3$ (Merck Life Science Pvt. Ltd., 99.99% Purity), TiO_2 (Merck Specialities Pvt. Ltd., 99.95% Purity), Y_2O_3 (Loba Chemie Pvt. Ltd., 99.9% Purity) originated from China.

2.2. Methods

Each of the materials was weighed exactly as needed, combined with the appropriate quantity of ethyl alcohol, and then pulverized for 20 h in a ball mill (G91-e.J. Payne, UK). The slurry was then put into a biker and dried for 24 h in a dryer (JISICO, J-s300S, Japan). The powders lasted 03 h in a mortar and pestle after drying. The mixes were then calcined for 02 h in an air-filled furnace at 1000 °C in an alumina crucible (Nabertherm GMBH, UK). A pellet press (Retsch Pellet Press PP 25) was subsequently employed to form the powder. The tablets were required to be shaped under 2.5 tons of compression. The tablets were then sintered in an air furnace for 2.5 h at 1250 °C (see Fig. 1). (Nabertherm GMBH, UK). A scanning electron microscope (ZEISS-EVO 18, UK) was applied to examine the structural characteristics of the sintered samples. To test the phase identification, X-ray diffraction (XRD; Bruker D8 Advanced, Germany) was used. The FULLPROF program was used to refine the structure. The impedance analyzer (Wayne Kerr 6500B series, UK) was used to test the room temperature (RT) dielectric constant with variable frequency.

3. Results and discussion

3.1. X-ray diffraction

The analysis of $BaTiO_3$ with varied dopant concentrations depicts the increase of the lattice parameter. At ambient temperature, XRD patterns in the 2-theta range of (20°–90°) are determined. A comparison of BCT and BCYT sample XRD patterns is illustrated in Fig. 2. The entire XRD patterns show the reducing calcium and yttrium peaks, as well as the generation of the $BaTiO_3$ peaks. The

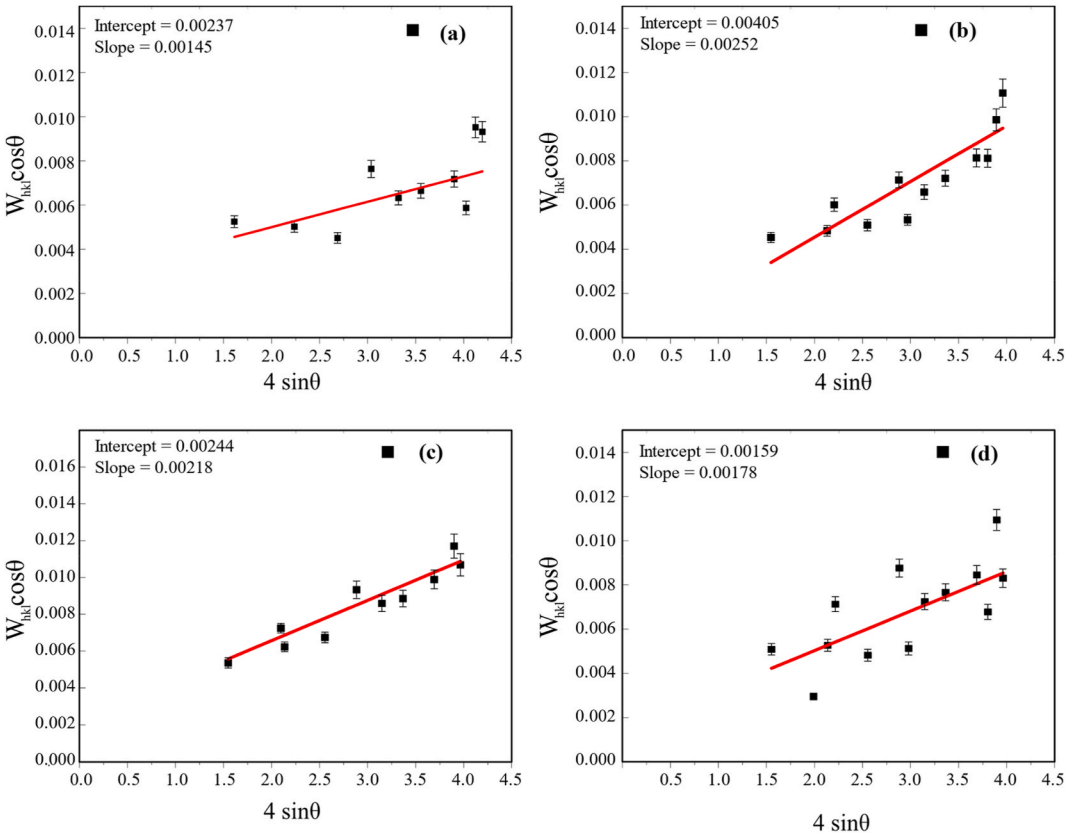

Fig. 5. Williamson and Hall (W–H) analysis of (a) BCT, (b) BCY_1T, (c) $BCY_{1.5}T$ and (d) BCY_2T ceramics.

Fullprof Suite's toolbar is used to investigate these diffraction angles to demonstrate the crystal's symmetry [31], as shown in Fig. 4. With its peaks, the cubic structure of the P m −3 m space group of BCT crystal and the tetragonal structure of the P4mm space group of BCYT crystal can be found in the XRD patterns. The XRD of the sintering sample shows an extra peak of calcium titanate in the BCT and BCY_1T samples, which matches JCPDS File No. 42–0535 [13]. Afterwards, when yttrium is started to be added at BCYT, the calcium titanate phase has begun to be demolished. Eventually, in $BCY_{1.5}T$, there is no secondary phase. Therefore, the existence peaks of $BCY_{1.5}T$ fully match those of $BaTiO_3$ (JCPDS file No. 05–0626). Further, when the amount of Y^{3+} increases in BCY_2T, the secondary phase YTi_2O_6 (JCPDS file No. 00-047-1786) is created because some of the Y^{3+} ions tend to take up A-sites along with B-sites. More oxygen vacancies arise in the second stage as Y^{3+} tends to replace A-site ions (Ba^{2+}). In the case of higher compositions of yttrium, such as BCY_2T, a minor decrease in the c/a ratio was observed [32]. Furthermore, as illustrated in Table 2, aliovalent substitutions lead to a lattice distortion [31]. The fullprof refinement values and lattice parameters are given in Table 1. Debye-Scherer formula [31] is implemented to compute the crystallite size (τ) using the maximum intense peak (110). The crystallite size and crystallinity are exhibited in Table 3. The variation in the sharpness of (110) diffraction peaks at 30°–32° is represented in Fig. 3 (a). With the increase in yttrium content, the peak shifts to the lower angle at 32° due to the atomic size factor [22]. Following Williamson and Hall (W–H), the main factors contributing to the enlargement of diffraction peak regions are distortion and strain on the lattice in the component triggered by a crystallite imperfection [33,34]. The W–H diagrams of Y-BCT samples are displayed in Fig. 5. The Williamson-Hall (W–H) method is a commonly employed methodology in the field of ceramics to investigate the influence of strain on the dimensions of crystallites. The presence of lattice strain within a crystalline structure can result in the broadening of X-ray diffraction (XRD) peaks. Peak broadening analysis is used in the W–H method to find out the size of the crystallites and the strain in the crystal lattice. The W–H plot depicted in Fig. 5 (c) indicates that the line dispersions exhibit predominantly isotropic behavior. This observation illustrates the isotropic nature of the diffraction domain, with the additional presence of dopants contributing to the macrostrain [35]. In Fig. 5 (d), due to the existence of secondary phases, the sharpness of FWHM has declined. Moreover, the values do not coincide with the line, and the highest deviation is observed. It has been found that the existence of lattice strain inside the structure had an impact on the placement and peak widening in the XRD pattern. The strain in the lattice is brought on by the difference in ionic radii between the host ions and the dopant ions [36]. Lattice parameters are increased and the location of the peak changes to a lower 2θ due to the inclusion of yttrium ions (0.101 nm) with relatively high ionic radii at the titanium (0.068) site [37]. Hence, C-axis expansion is observed, which is assured by the lattice parameter value mentioned in Table 2 [38]. The sample's tetragonality is attributed to the splitting of the (002) and (200) peaks at 44°–45° are of the yttrium-calcium co-doped sample shown in Fig. 3 (b). Yttrium is responsible for the emergence of tetragonal structures in all the BCYT samples. Further analysis has revealed that with a

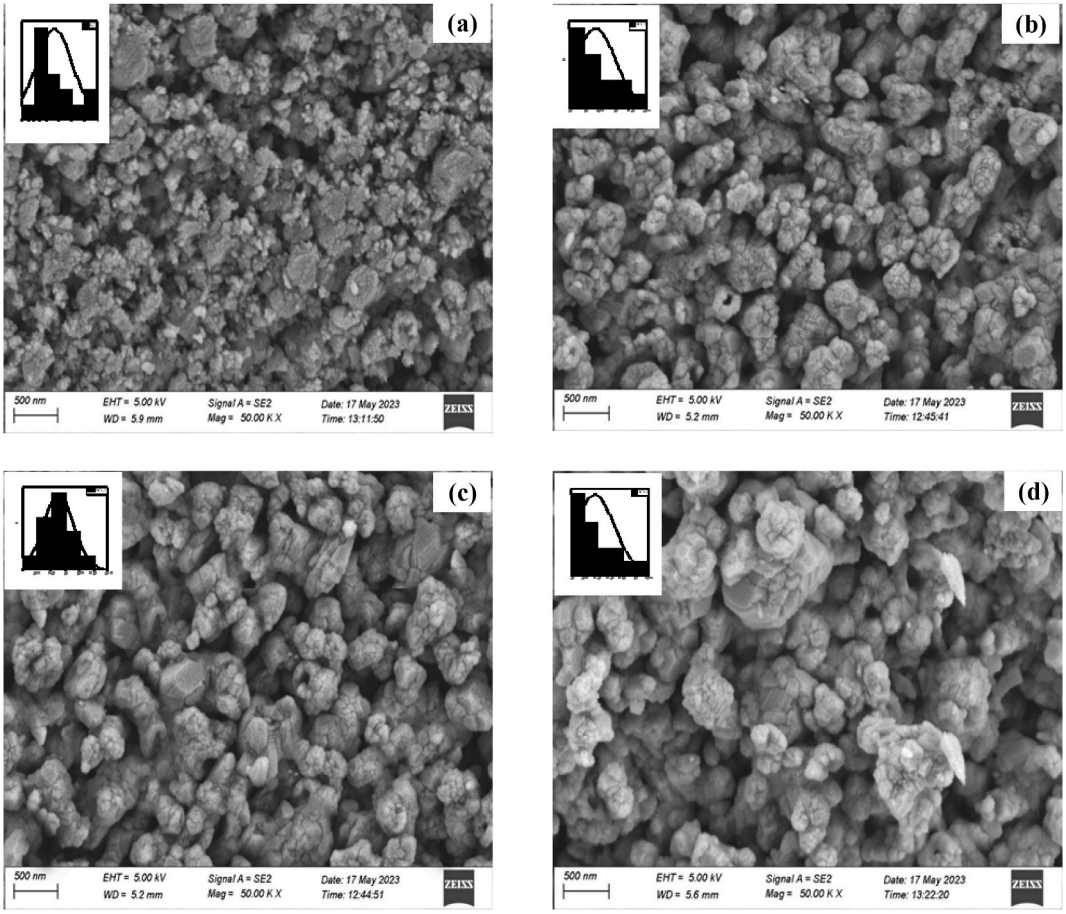

Fig. 6. Surface microstructures of (a) BCT, (b) BCY_1T, (c) $BCY_{1.5}T$ and (d) BCY_2T ceramics at a magnification of × 50.00K.

higher concentration of yttrium doping, the structure is distorted. Strain and dislocation density gradually increased [39], as expressed Table 2. Thus, tetragonality is lower. Moreover, the sample's tetragonality is attributed to the splitting of the (002) and (200) peaks at 44°–45°. Magnifying the particular peaks for the BCY_2T sample, peak broadening is allocated due to lattice distortion [18,19]. The degree of splitting and the difference in intensity between the (0 0 2) and (2 0 0) reflections show that the cubic and tetragonal phases existed at the same time [38]. The level of sharpness of those peaks shows that the samples are slightly moved towards cubic from tetragonal.

3.2. Scanning electron microscopy

The formation of liquid phase segregation in the grain boundaries and aberrant growth of grains is observed in Fig. 6. Furthermore, irregular grain development is seen. In the experimentation, we have attempted to demonstrate that the following issue can be prevented by RE doping [40]. We noticed the development of cubic-like grains with sharp edges and definite borders. However, certain grains' agglomerated dispersion was also discovered in the Y-BCT samples represented in Fig. 6 (b, c, d). These figures depict how the coarse grains were agglomerating as the boundaries between the finer grains gradually blurred. The average grain size of undoped BCT is less than that of Y-BCT samples. The variation in grain size may result from the second phase. The calcium titanate secondary phase present in BCT reduces grain size. In addition to the reduction in grain size, the inclusion of up to $y = 0.01$ in the BCT (BCY_1T) secondary phase emerges. Due to this factor, there are more imperfections between the grains, which can change how frequently the ceramic decays [41]. The calcium titanate secondary phase, whose existence is confirmed by XRD of the BCT sample, is responsible for the heterogeneity. The limited homogeneity of ceramic specimens shows that solid-state processes in the mixture of $BaCO_3$, $CaCO_3$, and TiO_2 particles cause a nonuniform distribution of Ba^{2+} and Ca^{2+} ions at the unit cell level. Microscopic chemical inhomogeneity caused by diffusional limits and delayed reaction kinetics limits the solubility of $CaTiO_3$ in $BaTiO_3$ when synthesized by the method. Inhomogeneity in composition is caused by solid-state solutions during calcination and sintering. The secondary phase during the solidification process might impede grain growth [42]. Particles of calcium titanate could act as barriers during the solidification process, limiting the movement of grain borders and halting the coarsening or growth of the grains into bigger sizes [43]. In the microstructure, it is evident that second phases appear together with the grain boundary liquid phase and precipitate in BCT. Subsequently, it

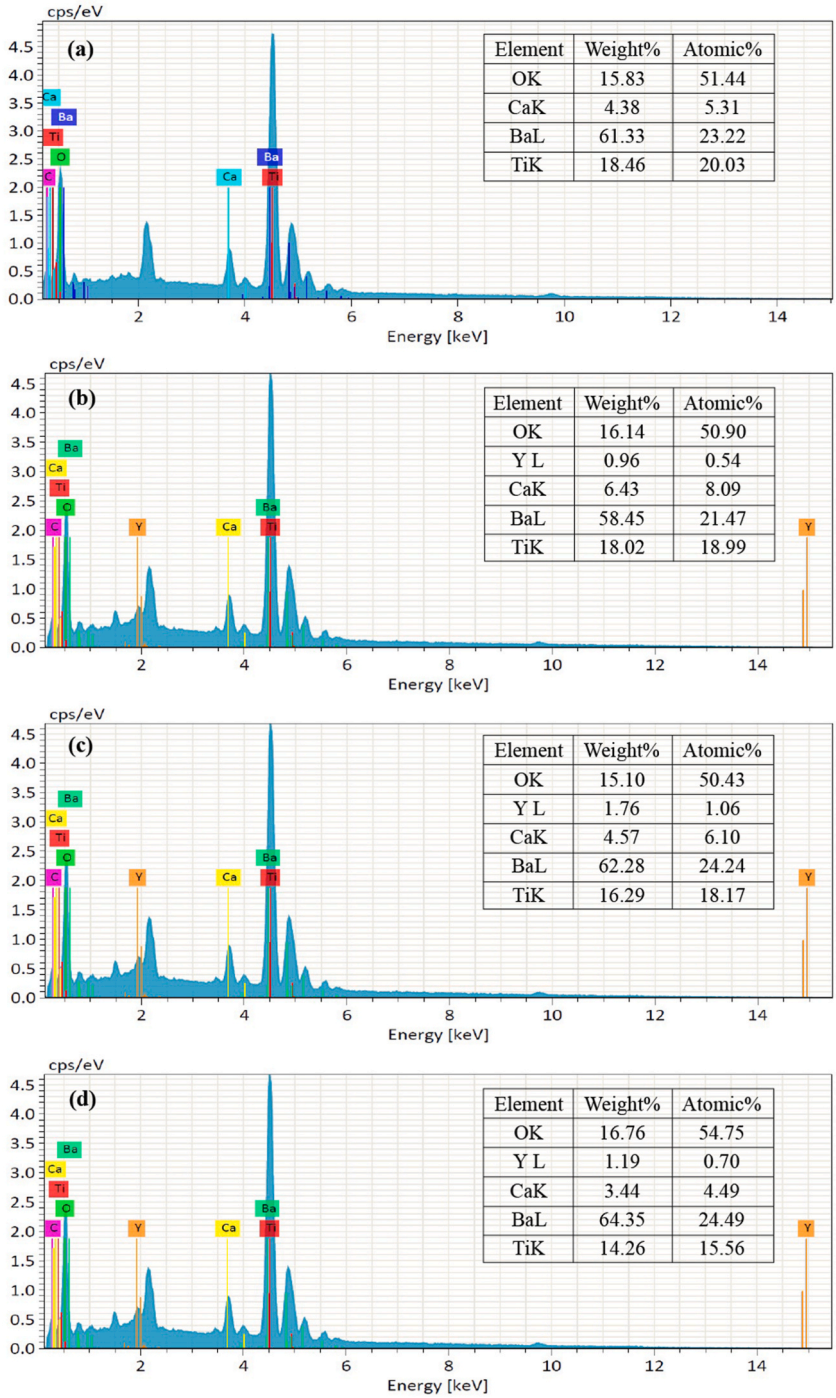

Fig. 7. Energy dispersive spectroscopy (EDS) spectra for (a) BCT, (b) BCY_1T, (c) $BCY_{1.5}T$ and (d) BCY_2T ceramics.

demonstrates that the grain distribution of Yttrium-doped BCT samples is more even, uniform, streamlined, and densely packed with a reduced porosity ratio than BCT. Barium vacancies aid in the densification process by diffusing more quickly than their ions. Due to improved diffusivity in the liquid phase of sintering, yttrium doping encourages densification [38]. Energy-dispersive spectroscopy (EDS) spectra for all the samples are illustrated in Fig. 7. While analyzing Energy Dispersive Spectroscopy (EDS), gold facilitates the detection and analysis of the distinctive peaks. When examining a sample, additional gold peaks in the 2nd region of the EDS spectrum are observed for different causes, such as X-ray fluorescence originating from the substrate or coating, as well as surface contamination or oxidation [42]. The BCY_2T sample has the largest grain size 29.28 nm, and they also have significant porosity which is mentioned in

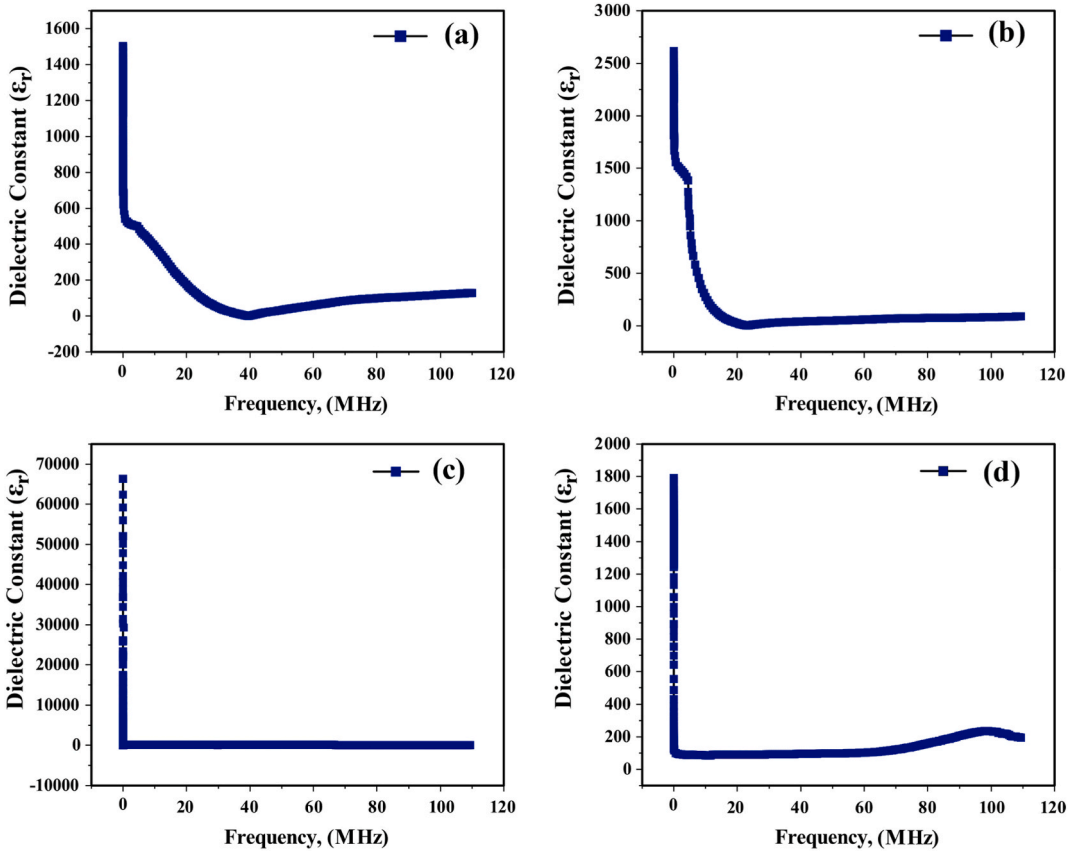

Fig. 8. Changes of dielectric constant with frequency for synthesized (a) BCT, (b) BCY_1T, (c) $BCY_{1.5}T$ and (d) BCY_2T ceramics.

Table 3.

3.3. Dielectric property

The relative dielectric constant observations of unmodified and yttrium-doped BCT ceramics as a function of frequency are displayed in Fig. 8. It has been claimed that the crystal structure and grain size had a significant impact on the solid solutions' dielectric characteristics [36]. With yttrium doping, the BCT lattice turned into a tetragonal structure from a cubic one, and the grain size increased. The Y-BCT samples exhibit greater densification with less porosity than BCT. When Yttrium ion is substituted in the Ti-site, the internal strain is increased. This causes the Ti^{4+} ions to be injected into the octahedral centers, which increases the polarization and hence the dielectric constant [44]. No additional secondary phase, homogeneous topology, and a compacted structure with less porosity made the $BCY_{1.5}T$ specimen more acceptable. The $BCY_{1.5}T$ exhibits an exceptional dielectric constant with an elevated rate of charge accumulation compared to other samples, as seen in Fig. 8 (c). Afterwards, with the addition of yttrium in the BCT lattice, a BCY_2T specimen was produced. Due to the larger atomic size of yttrium, which substituted titanium, higher strain caused defects like dislocations and abnormal grain growth. Consequently, the dielectric constant declaimed for BCY_2T, is represented in Fig. 8 (d). The low-frequency band (100–1000 Hz) demonstrates a substantial reduction in the dielectric constant. The capacitive responsiveness decreases at elevated frequencies when the charge carriers are more likely to be mobile and able to follow an AC frequency. Relaxation is necessary because interfacial polarization delays ion reversal with fluctuating fields at low frequencies [45]. To determine the Debye relaxation time, the following equation can be employed:

$$\tau = \varepsilon / (\sigma\ T) \tag{1}$$

where τ is the relaxation time, ε is the dielectric constant, σ is the electrical conductivity, and T is the temperature.

$$\gamma = 1/\tau = \sigma\ T / \varepsilon \tag{2}$$

It can be expressed using the Arrhenius law, which relates temperature to relaxation time.

$$\tau = \tau_0 \exp\ (Ea/k_B\ T) \tag{3}$$

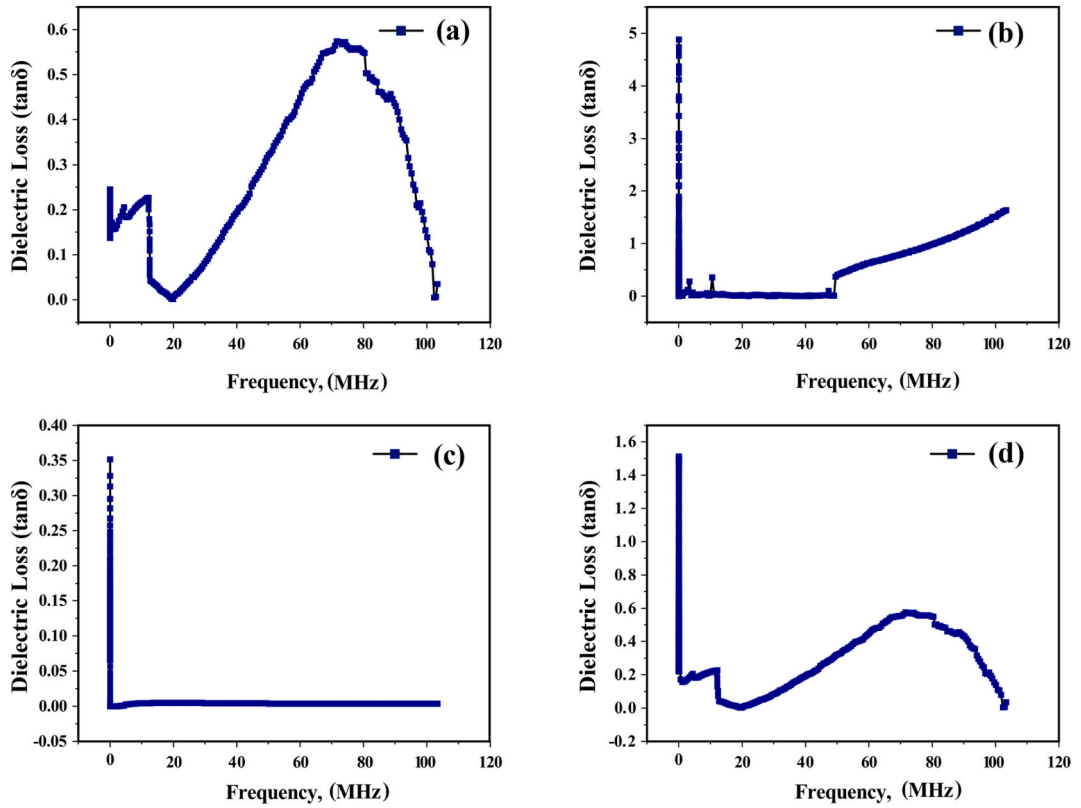

Fig. 9. Changes in dielectric loss tangent with frequency for synthesized (a) BCT, (b) BCY_1T, (c) $BCY_{1.5}T$ and (d) BCY_2T ceramics.

$$\ln \tau = \ln \tau_0 + (Ea/k_B)\ (1/T) \quad (4)$$

where τ_0 is a pre-exponential factor, Ea is the activation energy, k_B is the Boltzmann constant, and T is the temperature.

The Barium site is occupied by Ca ions. The intrinsic disorder effect has been brought about by the substitution of A or B cation positions in the ABO_3 structure. It is found that the dielectric constant gradually decreases when yttrium doping approaches BCY_2T. Oxygen vacancies contribute to the deficiency charge when the Y^{3+} cation is aliovalently incorporated at the Ti site, with the reaction

$$Y_2O_3 + 2BaO \rightarrow 2Ba_{Ba} + 2Y'_{Ti} + 5O_O + V''O \quad (5)$$

The $BCY_{1.5}T$ has the highest value of maximum dielectric constant, which could be attributed to the presence of well-developed grains, as depicted in Fig. 6 (c). The presence of well-developed grains facilitates the movement of domain walls, resulting in an increased dielectric constant. Furthermore, the augmentation in dielectric constant could also be understood as a result of the subsequent factor. Due to the fact that sintering is conducted in an ambient air environment, there is a potential for reoxidation to occur in the vicinity of the grains during the cooling phase [40]. Consequently, the lattice structure has the capacity to absorb oxygen from the surrounding atmosphere. The process of reoxidation leads to the formation of a robust insulating layer surrounding the grains, which exhibits increased bulk resistance. The disparity in conductivity between the bulk and grain boundaries arises from the fact that the grain boundary exhibits higher resistance and capacitance compared to the grain interior. Consequently, this leads to the accumulation of surface charge and an increase in interfacial polarization, ultimately resulting in an elevation of the dielectric constant [23].

The observed significant rise in dielectric loss could be attributed to the accelerated mobility of charge carriers resulting from flaws or vacancies present in the sample. The dielectric loss tends to go up, and this may be caused by the creation of the second phase in BCY_1T during the sintering process, which determines the dielectric characteristics [46,32], which is shown in Fig. 9 (b). The second phase of YTi_2O_6 corresponding to titanium, was formed when Y_2O_3 was added to the $BaTiO_3$ ceramics [47]. The YTi_2O_6 phase's higher oxygen ionic conductivity will speed up the electro-migration of oxygen vacancies, which will lead to resistance degradation [48]. Ionic defect structures are typically in partially frozen-in states after sintering and during the cooling process, retaining the high-temperature defect structures. As a result, the phase present in the dielectric layer of the ceramic capacitor based on $BaTiO_3$ may have a substantial impact on the dependability of insulating resistance by facilitating the electro migration of oxygen vacancies [49]. The XRD pattern verifies the existence of BCY_1T ceramic second phases. The elevated carrier mobility of the ceramics can be attributed to their exceptionally porous microstructure. Perhaps the amount of porosity is 47% for BCY_1T, which is higher than other Y-BCT samples. This phenomenon was also responsible for higher dielectric loss. Therefore, the production of cation-rich and/or oxygen-deficient precipitates at the grain boundaries (i.e., functioning as conduction routes) is responsible for the high electrical conductivity of the BCY_1T ceramic [50]. It is well known that charge trapping defects, such as oxygen vacancies, that preferentially

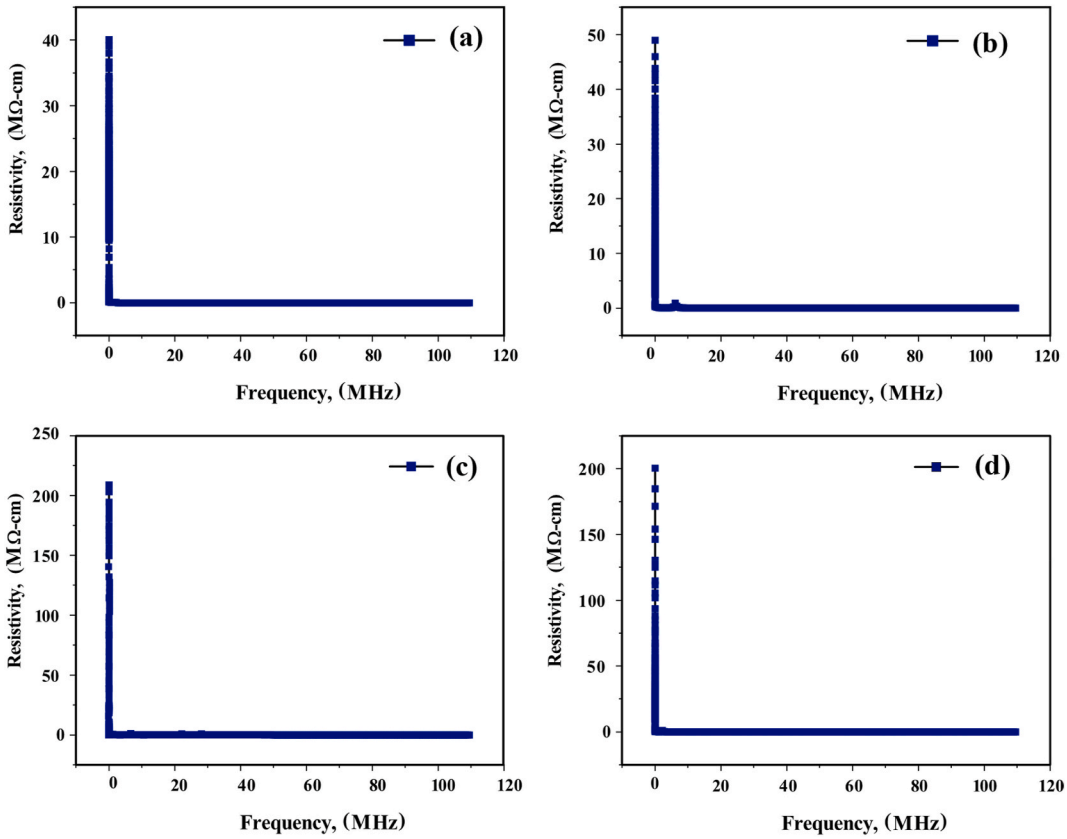

Fig. 10. Variation of resistivity with frequency for synthesized (a) BCT, (b) BCY_1T, (c) $BCY_{1.5}T$ and (d) BCY_2T ceramics.

cluster at grain boundaries offer preferred percolation pathways for leakage current [41]. As a result, the grain boundaries would serve as electron transport conduction routes. The presence of loosely bound oxygen vacancies may move to the grain boundary and contribute to the space charge's polarization; internal stress is higher for BCY_1T due to the second phase [51,52].

3.4. Electrical property (frequency dependence of AC resistivity and conductivity)

The resistivity profile of the samples manufactured is shown in Fig. 10, which illustrates the way frequency-aligned dependence on Y^{3+} concentration at ambient temperature works. The concentrations of Y^{3+} doping at substantial levels reveal significant upward resistivity with the comparison of BCT. Resistivity has a sharply declining pattern up to the 110 KHz frequency range before being frequency-independent. It can be explained by the fact that hopping random charge carriers in the low-frequency band reduce resistivity [23]. Consequently, the occurrence of an additional phase in the dielectric substance of a ceramic capacitor developed on the BCY_1T substrate may significantly affect the dependability of insulation resistance by exposing an easy route for oxygen vacancies to migrate electrochemically, which is responsible for the higher electrical conductivity and less resistance [53]. According to reports, the secondary phase possesses an oxygen ion conductivity that is 4–12 times greater than that of undoped $BaTiO_3$ [54]. $y = 0.01$ (BCY_1T) sample has the highest electrical conductivity 2.04×10^{-7} S/m than other Y-BCT samples, which is represented in Fig. 11 (b). The resistivity and conductivity value at room temperature is also mentioned in Table 4. The complexity of conductivity in dielectrics is widely acknowledged. Firstly, in the BCY_1T sample, conductivity stays nearly constant, resembling a plateau. The most common mechanisms probably charge compensation via cation vacancies [55]. The conductivity improves continuously while the electron mobility stays constant. The BCY_1T sample consistently exhibits higher electrical conductivities than the other samples. The Y^{3+} dissolution kinetics might also be reflected in the slope of rising conductivity [56]. Furthermore, conductivities arise from a combined mechanism of cation and electron vacancy compensation, wherein the electron compensation occurs gradually. The inclusion of pores within BCT sample has the potential to augment its surface area, thereby facilitating an increase in the quantity of charge carriers that are accessible for participation in the electric current. This phenomenon results in an elevation of the material's conductivity and a concomitant reduction in resistance [57]. The existence of flaws, vacancies, imperfections, and variations in lattice characteristics has an impact on it. From SEM analysis it was reported that the BCT specimen exhibits reduced grain size and possesses a microstructure characterized by porosity [56]. The overall conductivity in the sintered ceramic of $BCY_{1.5}T$ is influenced by the occupancy of the Y^{3+} site; Y^{3+} turns into an acceptor-cation and self-compensates. Its more noticeable impact on conductivity has made it possible for Y^{3+} to dissolve more readily, which in turn has led to decreased conductivity as a result of self-compensation [58]. Hence the highest

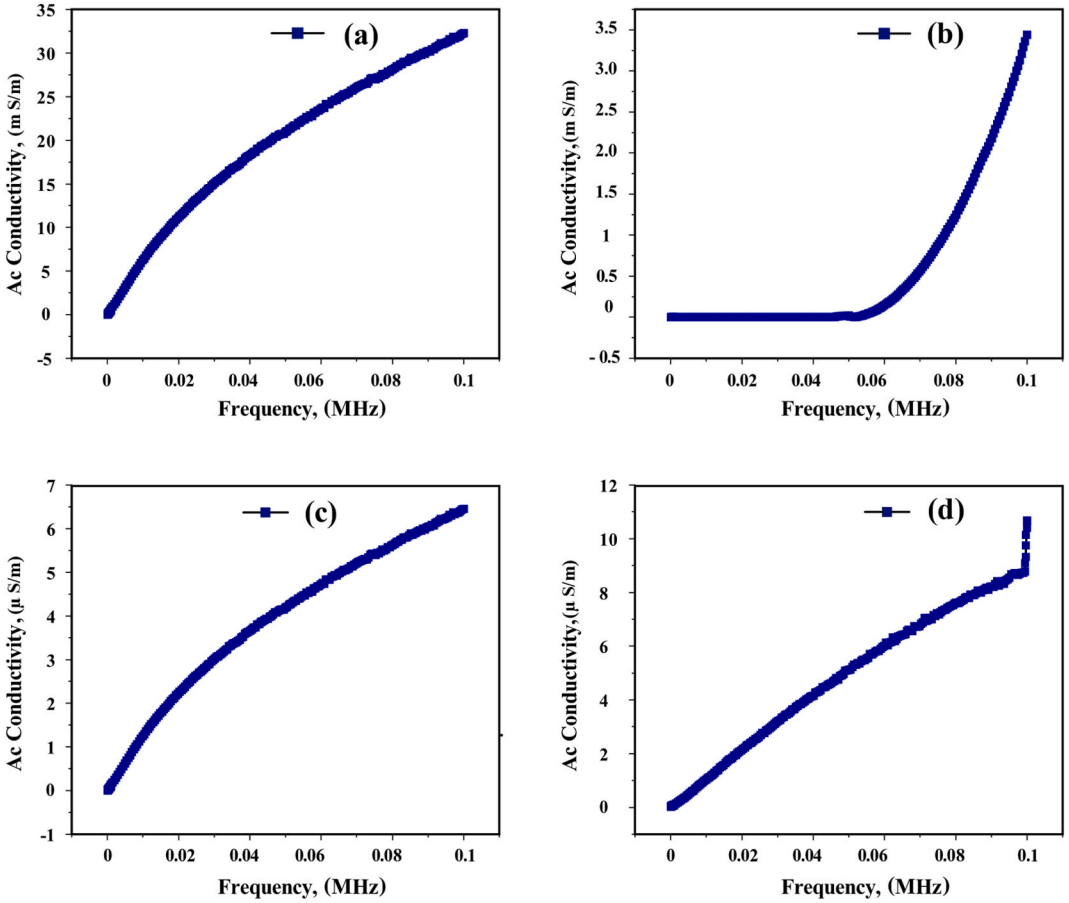

Fig. 11. Variation of AC conductivity with frequency of synthesized (a) BCT, (b) BCY_1T, (c) $BCY_{1.5}T$ and (d) BCY_2T ceramics.

Table 4
Dielectric properties and reciprocal of relaxation time, (γ) value of BCT, BCY_1T, $BCY_{1.5}T$ And BCY_2T ceramics at temperature 300K.

Sample	Dielectric Constant (κ) at 1000 k Hz	Dielectric Loss (tanδ)	Electrical conductivity, σ (S/m)	$\gamma = \sigma T/\varepsilon$	Resistivity (Ω-cm)
(BCT)	113	0.138	1.10×10^{-5}	2.52×10^{-6}	9.00×10^{4}
(BCY_1T)	238	0.440	2.04×10^{-7}	4.09×10^{-8}	4.00×10^{7}
($BCY_{1.5}T$)	2150	0.029	4.95×10^{-9}	2.14×10^{-11}	5.00×10^{8}
(BCY_2T)	1244	0.072	2.49×10^{-8}	4.17×10^{-9}	4.00×10^{8}

resistivity was attained for $BCY_{1.5}$ T. Fig. 12 displays the Nyquist plots, which depict the relationship between the imaginary portion of the impedance (Z″) and the real part of the impedance (Z′), throughout a broad frequency spectrum. These plots serve as a means of examining the impedance qualities. It is important to observe that the complex impedance spectrum had a linear trend with a significant gradient, which signifies the sample's insulating characteristics [59]. Among the several options considered, $BCY_{1.5}T$ exhibited the highest degree of insulation due to its pronounced elevation in the plotted line [60]. The BCY_1T sample demonstrated a semicircular response when subjected to low frequencies, whereas at higher frequencies, it displayed a little curvature before transitioning into a linear behavior [61]. In contrast, $BCY_{1.5}T$ did not demonstrate semicircle behavior when subjected to low frequencies. However, the three samples exhibited comparable behavior when exposed to high frequencies [35,58].

4. Conclusions

In conclusion, BCYT- (00, 0.10, 0.15, and 0.20) ceramics were successfully prepared by solid-state method. Yttrium doping in barium titanate ceramics can supplement the positive effects of calcium doping and mitigate some of its negative effects. This comprehensive investigation shows that yttrium doping plays a significant role in modifying the structural stability, phase stability, and chemical compatibility of barium calcium titanate ceramics.

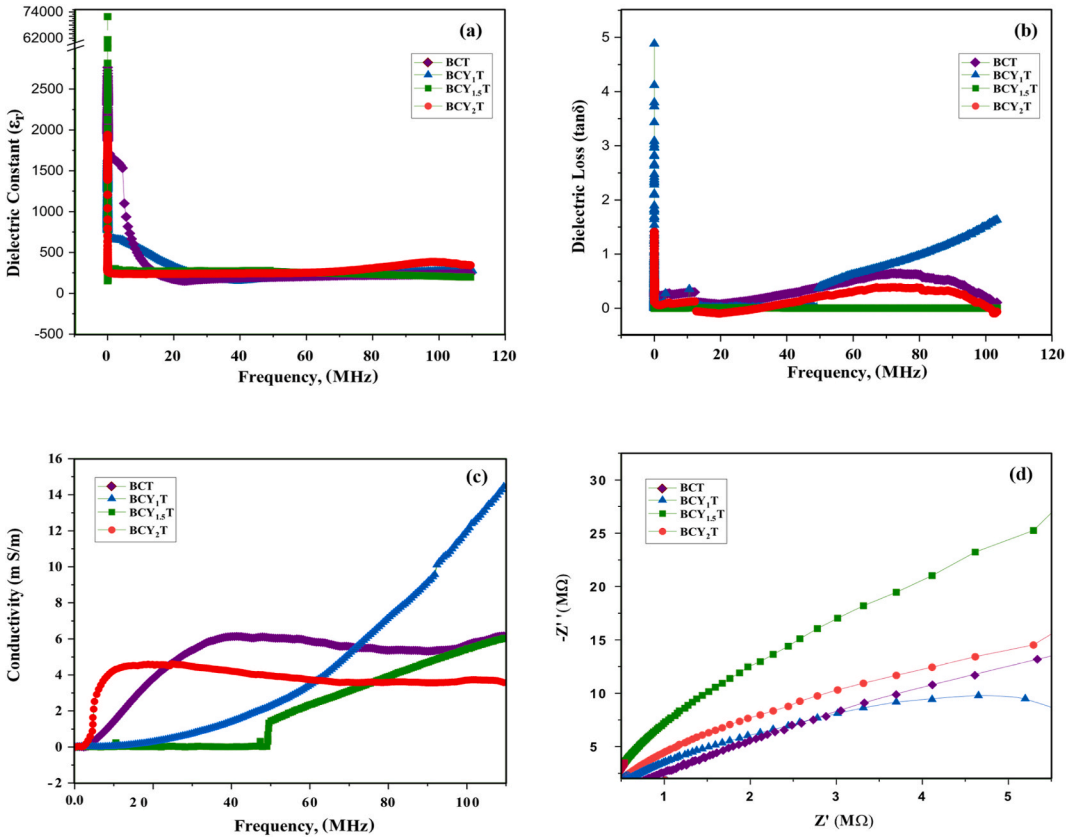

Fig. 12. Frequency dependence of (a) dielectric constant, (b) dielectric loss, (c) electrical conductivity, and (d) Nyquist (Z'' vs. Z') plot for synthesized BCT, BCY_1T, $BCY_{1.5}T$ and BCY_2T ceramics.

- The cubic structure of the P m −3 m space group of BCT crystal and the tetragonal structure of the P4mm space group of BCYT crystal are found in the XRD patterns. Crystallite size, grain size, strain and dislocation density increased with the inclusion of yttrium because of the larger ionic radius of yttrium than titanium.
- The calcium titanate secondary phase present in BCT suppresses grain size 18.48 nm, has higher electrical conductivity 1.10×10^{-5} S/m and less resistivity 9×10^4 Ω-cm. $BCY_{1.5}T$ exhibits an exceptional dielectric constant with an elevated rate of charge accumulation compared to other samples.
- The ranges of the dielectric constant were standardized for the y = 0.01 (BCY_1T) specimen to demonstrate the declining dependency with frequency to evaluate the particular influence of the secondary phase on the dielectric characteristics.
- The higher oxygen ionic conductivity of the YTi_2O_6 phase will speed up the electro-migration of oxygen gaps, which will lower the resistance. $BCY_{1.5}$ T was found to have the highest resistance. So, the presence of an extra phase in the dielectric material of a ceramic capacitor made on a BCY_1T substrate can have a big effect on how reliable the insulation resistance is. This is because it makes it easy for oxygen vacancies to move electrochemically, which is what gives Y-BCT ceramics their higher electrical conductivity and lower resistance.

The results of this work reveal new avenues for investigation and the creation of novel functional materials with specific features for a range of technological applications.

CRediT authorship contribution statement

Hasnat Jahan Sumona: Writing – original draft, Methodology, Investigation, Formal analysis, Conceptualization. **Abdullah Al Mahmood:** Writing – review & editing, Supervision, Methodology. **M. Bodiul Islam:** Writing – review & editing. **Jahid Hasan Kasem:** Investigation, Formal analysis. **M.S. Rahman:** Resources.

Declaration of competing interest

The authors declare that they have no known competing financial interests or personal relationships that could have appeared to influence the work reported in this paper.

Acknowledgement

The authors sincerely acknowledge the supports provided by the laboratories in the Department of Glass & Ceramic Engineering, Rajshahi University of Engineering & Technology (RUET), and Bangladesh Council of Scientific and Industrial Research (BCSIR), Dhaka, Bangladesh.

References

[1] Vojislav V. Mitic, Zoran S. Nikolic, Vladimir B. Pavlovic, "Influence of rare-earth dopants on barium titanate ceramics microstructure and corresponding electrical properties,", J. Am. Ceram. Soc. (25042) (2010) 132–137, https://doi.org/10.1111/j.1551-2916.2009.03309.x.
[2] S.M.A. Kader, D.E.J. Ruth, M.V. Gajendra, M. Muneeswaran, Investigations on the effect of Ba and Zr co-doping on the structural, thermal, electrical and magnetic properties of $BiFeO_3$ multiferroics, Ceram. Int. 43 (2016), https://doi.org/10.1016/j.ceramint.2017.08.104.
[3] X. Han, et al., Excellent dielectric properties and enhanced temperature stability of $CaZrO_3$ - modified $BaTiO_3$ ceramic capacitors, J. Mater. Sci. Mater. Electron. 31 (16) (2020) 13088–13094. https://link.springer.com/article/10.1007/s10854-020-03859-w.
[4] P.K. Panda, B. Sahoo, V. Sureshkumar, E.D. Politova, Effect of Zr^{4+} on piezoelectric , dielectric and ferroelectric properties of barium calcium titanate lead-free ceramics, Journal of Advanced Dielectrics 11 (6) (2021) 1–9, https://doi.org/10.1142/S2010135X21500247.
[5] J. Park, Y. Lee, K. Kim, Y. Kim, Nuclear instruments and methods in physics research B structural study of Ca doped barium titanate, Nucl. Instrum. Methods Phys. Res. B 284 (2012) 44–48, https://doi.org/10.1016/j.nimb.2011.07.107.
[6] V. Sreenivas, D.K. Pradhan, B.C. Riggs, D.B. Chrisey, R.S. Katiyar, Investigations on structure , ferroelectric , piezoelectric and energy storage properties of barium calcium titanate (BCT)ceramics, J. Alloys Compd. 584 (2014) 369–373, https://doi.org/10.1016/j.jallcom.2013.09.108.
[7] L. Kadira, Dielectric study of calcium doped barium titanate $Ba_{1-x}Ca_xTiO_3$ ceramics, Int. J. Phys. Sci. 11 (6) (2016) 71–79, https://doi.org/10.5897/IJPS2015.4415.
[8] R. Varatharajan, S.B. Samanta, R. Jayavel, C. Subramanian, A. V Narlikar, P. Ramasamy, Ferroelectric characterization studies on barium calcium titanate single crystals, Mater. Char. 45 (2000) 89–93, https://doi.org/10.1016/S1044-5803(00)00053-X.
[9] V. Paunovic, L. Živkovic, L. Vracar, V. Mitic, M. Miljkovic, The effects of additive on microstructure and electrical properties of $BaTiO_3$ ceramics, Serbian Journal of Electrical Engineering 1 (3) (2004) 89–98, https://doi.org/10.2298/SJEE0403089P, 1(3).
[10] F. V Motta, et al., Preparation and characterizations of Ba0.8Ca0.2TiO3 by complex polymerization method (CPM), J. Alloys Compd. 465 (2008) 452–457, https://doi.org/10.1016/j.jallcom.2007.10.107.
[11] T. Zaman, K. Islam, A. Rahman, A. Hussain, A. Matin, Mono and co-substitution of Sr^{2+} and Ca^{2+} on the structural, electrical and optical properties of barium titanate ceramics, Ceram. Int. 45 (8) (2019) 10154–10162, https://doi.org/10.1016/j.ceramint.2019.02.064.
[12] U. Federal, R. De Pernambuco, A. Paula, D.A. Marques, R. Tranquilin, C.A. Paskocimas, "Effect of different starting materials on the synthesis of $Ba_{0.8}Ca_{0.2}TiO_3$", Journal of Advanced Ceramics 4 (1) (2015) https://doi.org/10.1007/s40145-015-0134-4.
[13] S. Jayanthi, T.R.N. Kutty, Extended phase homogeneity and electrical properties of barium calcium titanate prepared by the wet chemical methods, Mater. Sci. Eng., B 110 (2004) 202–212, https://doi.org/10.1016/j.mseb.2004.03.008.
[14] Z.Q. Zhuang, M.P. Harmer, D.M. Smyth, R.E. Newnham, The effect of octahedrally-coordinated calcium on the ferroelectric transition of $BaTiO_3$, Mater. Res. Bull. 22 (c) (1987), https://doi.org/10.1016/0025-5408(87)90296-0.
[15] A. Alshoaibi, M.B. Kanoun, B.U. Haq, S. Alfaify, S. Goumri-said, Insights into the impact of yttrium doping at the Ba and Ti sites of BaTiO3 on the electronic structures and optical properties :AFirst-PrinciplesStudy, ACS Omega 25 (2020) 15502–15509, https://doi.org/10.1021/acsomega.0c01638.
[16] B. Ca, et al., Improved dielectric and energy storage properties in $_{(1-x)}\ BaTi_{0.80}Zr_{0.20}O\text{-}_xBa_{0.70}Ca_{0.30}Ti_{0.99}Fe_{0.01}O_3$ ceramics near morphotropic phase boundary, Mater. Lett. 2100062 (2021) 1–9, https://doi.org/10.1016/j.matlet.2022.132126.
[17] Q. Zhang, W. Cai, Q. Li, R. Gao, G. Chen, Enhanced piezoelectric response of (Ba, Ca) (Ti, Zr) O_3 ceramics by super large grain size and construction of phase boundary, J. Alloys Compd. 794 (2019) 542–552, https://doi.org/10.1016/j.jallcom.2019.04.247.
[18] S.M.R.S.T. Som, Effect of Fe-ion implantation doping on structural and optical properties of CdS thin films, Appl. Phys. A 99 (2010) 837–842, https://doi.org/10.1007/s00339-010-5598-z.
[19] S. Sarangi, I.C. Tan, A. Brazdeikis, Magnetic imaging method based on magnetic relaxation of magnetic nanoparticles, J. Appl. Phys. 93926 (2009) (2012), https://doi.org/10.1063/1.3125460.
[20] D. Shan, Y.F. Qu, J.J. Song, Dielectric properties and substitution preference of yttrium doped barium zirconium titanate ceramics, Solid State Commun. 141 (2007) 65–68, https://doi.org/10.1016/j.ssc.2006.09.050.
[21] C. Fu, W. Cai, A comparative study on the structural, dielectric and multiferroic properties, Compos. Part B 166 (November 2018) (2019) 204–212, https://doi.org/10.1016/j.compositesb.2018.12.010.
[22] M.S. Silva, N.S. Ferreira, Effects of La doping on the structural and dielectric properties of barium-titanate ceramics, Adv. Mater. Res. 975 (2014) 36–41, https://doi.org/10.4028/www.scientific.net/AMR.975.36.
[23] S. Islam, N. Khatun, M.S. Hossain, Investigation of structural , dielectric and electrical properties of barium titanate ceramics Co-doped with bismuth and yttrium, Journal of Molecular and Engineering Materials 7 (2019) 2251–2381, https://doi.org/10.1142/S2251237319500060. October 2020.
[24] H. Muta, K. Kurosaki, S. Yamanaka, Thermoelectric properties of rare earth doped $SrTiO_3$, J. Alloys Compd. 350 (2003) 292–295, https://doi.org/10.1016/S0925-8388(02)00972-6.
[25] I.A. Velasco-davalos, A. Ruediger, J.J. Cruz-rivera, C. Gomez-yanez, Mechanical niobium doping in barium titanate electroceramics, J. Alloys Compd. 581 (2013) 56–58, https://doi.org/10.1016/j.jallcom.2013.06.187.
[26] A. Belous, V. Oleg, L. Kovalenko, D. Makovec, Redox processes in highly yttrium-doped barium titanate, J. Solid State Chem. 178 (2005) 1367–1375, https://doi.org/10.1016/j.jssc.2005.01.014.
[27] S. Kumar, V. Luthra, Journal of Physics and Chemistry of Solids Raman and infrared spectroscopic investigation of the effects of yttrium and tin co-doping in barium titanate, J. Phys. Chem. Solid. 154 (March) (2021) 110079, https://doi.org/10.1016/j.jpcs.2021.110079.
[28] J. Liu, G. Jin, Y. Chen, W. Xue, Properties of yttrium-doped barium titanate ceramics with positive temperature coefficient of resistivity and a novel method to evaluate the depletion layer width, Ceram. Int. 45 (5) (2019) 6119–6124, https://doi.org/10.1016/j.ceramint.2018.12.086.
[29] W. Cai, C. Fu, J. Gao, Z. Lin, X. Deng, Effect of hafnium on the microstructure , dielectric and ferroelectric, Ceram. Int. 38 (4) (2012), https://doi.org/10.1016/j.ceramint.2011.12.047.
[30] Young Soo Lim, Subramanian Sasikumar, Hae Won Lee, Competing effects of Ca doping on the phase transition and related properties in $(Ba_{1-x}Ca_x)(Ti_{0.95}Sn_{0.05})O_3$ ceramics, J. Korean Ceram. Soc. (2023) 0123456789, https://doi.org/10.1007/s43207-023-00341-1.
[31] M. Ganguly, et al., Characterization and rietveld refinement of A-site deficient lanthanum doped barium titanate, J. Alloys Compd. 579 (2013), https://doi.org/10.1016/j.jallcom.2013.06.104.
[32] P.A. Jha, A.K. Jha, Effects of yttrium substitution on structural and electrical properties of barium zirconate titanate ferroelectric ceramics, Curr. Appl. Phys. 13 (7) (2013) 1413–1419, https://doi.org/10.1016/j.cap.2013.04.032.
[33] A.M. Balakt, C.P. Shaw, Q. Zhang, Enhancement of pyroelectric properties of lead-free $_{0.94}Na_{0.5}Bi_{0.5}TiO_3\text{-}_{0.06}BaTiO_3$ ceramics by La doping, J. Eur. Ceram. Soc. (2016) 6–13, https://doi.org/10.1016/j.jeurceramsoc.2016.12.021.
[34] E. Hannachi, M.A. Almessiere, Y. Slimani, R.B. Alshamrani, G. Yasin, F. Ben Azzouz, Preparation and characterization of high-T c ($YBa_2Cu_3O_{7-\delta}$) 1-x/(CNTs) x superconductors with highly boosted superconducting performances, Ceram. Int. 47 (2021) 23539–23548, https://doi.org/10.1016/j.ceramint.2021.05.071.

[35] R. Ravanamma, et al., Yttria activated lanthanum -barium titanate ceramic electrode for fast charging supercapacitor applications, J. Mol. Struct. 1294 (P2) (2023) 136352, https://doi.org/10.1016/j.molstruc.2023.136352.

[36] M.H.M. Akmal, A.R.M. Warikh, U.A.A. Azlan, M.A. Azam, Structural evolution and dopant occupancy preference of yttrium-doped potassium sodium niobate thin films, J. Electroceram. (2016) 3–10. https://link.springer.com/article/10.1007/s10832-016-0039-9.

[37] S. Kumar, V. Shrivastava, O.P.T. Vandna, Cumulative effect of yttrium and tin co-doping on the structural and ferroelectric properties of sol – gel derived barium titanate, J. Sol. Gel Sci. Technol. 105 (2023) 304–314, https://doi.org/10.1007/s10971-022-05910-0.

[38] H.K.A. Renteria-marquez, N.D. Love, Y. Lin, D. Islam, L.A. Chavez, Fabrication of bulk piezoelectric and dielectric $BaTiO_3$ ceramics using paste extrusion 3D printing technique, Journal of Americal Ceramic Society 102 (6) (2018) 3685–3694, https://doi.org/10.1111/jace.16242.

[39] S. Chandramohan, et al., Modifications in structural and optical properties of Mn-ion implanted CdS thin films, Appl. Surf. Sci. 256 (2009) 465–468, https://doi.org/10.1016/j.apsusc.2009.07.015.

[40] A.P.A. Moraes, et al., Structural and optical properties of rare earth – doped $(Ba_{0.77}Ca_{0.23})$ 1 − x (Sm , Nd , Pr , Yb) $xTiO_3$ Structural and optical properties of rare earth – doped $(Ba_{0.77}Ca_{0.23})$(1-x)(Sm, Nd, Pr, Yb)(x)TiO_3, J. Appl. Phys. (2011) 124102, https://doi.org/10.1063/1.3594710, 0–8.

[41] Y. Slimani, et al., Study on the addition of SiO_2 nanowires to $BaTiO_3$: structure, morphology, electrical and dielectric properties, J. Phys. Chem. Solid. 156 (May) (2021) 110183, https://doi.org/10.1016/j.jpcs.2021.110183.

[42] V. Bijalwan, P. Tofel, V. Holcman, Grain size dependence of the microstructures and functional properties of $(Ba_{0.85}Ca_{0.15-x}Ce_x)(Zr_{0.1}Ti_{0.9})O_3$ lead-free piezoelectric ceramics, J. Asian Ceram. Soc. (2020) 1–10, https://doi.org/10.1080/21870764.2018.1539211.

[43] M. Özen, M. Mertens, F. Snijkers, P. Cool, Hydrothermal synthesis and formation mechanism of tetragonal barium titanate in a highly concentrated alkaline solution, Ceram. Int. (2016) 1–9, https://doi.org/10.1016/j.ceramint.2016.03.234.

[44] M. Society, Effect of yttrium doping in barium zirconium titanate ceramics : a structural, impedance, modulus-spectroscopy study, Metall. Mater. Trans. 44 (2013) 4296–4309. https://link.springer.com/article/10.1007/s11661-013-1770-3.

[45] S. More, R. Dhokne, S. Moharil, Dielectric relaxation and electric modulus of polyvinyl alcohol Zinc oxide composite films, Mater. Res. Express 4 (2018), https://doi.org/10.1016/j.vacuum.2018.11.051.

[46] T. Badapanda, C.V.R.G. Univeristy, S.K. Rout, S. Panigrahi, T.P. Sinha, Dielectric behavior of yttrium doped barium-zirconium-titanate ceramics, J. Kor. Phys. Soc. 55 (141) (2009) 65–68, https://doi.org/10.1016/j.ssc.2006.09.050.

[47] H. Search, C. Journals, A. Contact, M. Iopscience, I.P. Address, Relationship between the evolutions of the microstructure and semiconductor properties of yttrium-doped barium titanate ceramics, Ceram. Int. 345403 (2018) 12–86, https://doi.org/10.1016/j.ceramint.2018.12.086.

[48] S. Yoon, Y. Park, J. Hong, D. Sinn, Effect of the pyrochlore $(Y_2Ti_2O_7)$ phase on the resistance degradation in yttrium-doped $BaTiO_3$ ceramic capacitors, J. Mater. Res. (May 2014) (2007) 2539–2543, https://doi.org/10.1557/jmr.2007.0326.

[49] M.I.A.A. Maksoud, et al., Advanced Materials and Technologies for Supercapacitors Used in Energy Conversion and Storage : a Review, Springer International Publishing, 2020 0123456789, https://doi.org/10.1007/s10311-020-01075-w.

[50] M.P. Hörlein, A.K. Opitz, J. Fleig, On the variability of oxygen exchange kinetics of platinum model electrodes on yttria stabilized zirconia, Solid State Ionics 247–248 (2013) 56–65, https://doi.org/10.1016/j.ssi.2013.04.023.

[51] S. Kumar, O. Thakur, V. Luthra, Modulating the effect of yttrium doping on the structural and dielectric properties of barium titanate, Phys. Status Solidi 215 (7) (2018) 1–8, https://doi.org/10.1016/j.heliyon.2022.e10529, 1700710.

[52] M. Aghayan, A.K. Zak, M. Behdani, A.M. Hashim, Sol – gel combustion synthesis of Zr-doped $BaTiO_3$ nanopowders and ceramics : dielectric and ferroelectric studies, Ceram. Int. 40 (2014) 16141–16146, https://doi.org/10.1016/j.ceramint.2014.07.045.

[53] V. Paunović, L. Živković, V. Mitić, Influence of rare-earth additives (La, Sm and Dy) on the microstructure and dielectric properties of doped $BaTiO_3$ ceramics, Sci. Sinter. 42 (1) (2010) 69–79, https://doi.org/10.2298/SOS1001069P.

[54] H. Yoo, C. Song, D. Lee, $BaTiO_3 - \delta$: defect structure, electrical conductivity, chemical diffusivity, $BaTiO_3 - \delta$: defect structure, electrical conductivity, J. Electroceram. 8 (1) (2014) 5–36, https://doi.org/10.1023/A:1015570717935. July 2002.

[55] D. Makovec, Z. Samardz, M. Drofenik, Solid solubility of Holmium , yttrium , and Dysprosium in $BaTiO_3$, J. Am. Ceram. Soc. 1329 (10167) (2004) 1324–1329, https://doi.org/10.1111/j.1151-2916.2004.tb07729.x.

[56] H. Wang, et al., The dielectric properties of alternately doped Ba1-xSrxTiO3 films with different Ba/Sr ratios with different Ba/Sr ratios, Ceram. Int. 45 (2019) 8300–8304, https://doi.org/10.1016/j.ceramint.2019.01.136, r.

[57] Z. Cai, et al., High-temperature lead-free multilayer ceramic capacitors with ultrahigh energy density and efficiency fabricated via two-step sintering, J. Mater. Chem. A (2019) 14575–14582, https://doi.org/10.1039/C9TA04317A.

[58] R. Rallapalli, Niobium oxide-activated yttrium barium titanate nanorod structured ceramics for energy storage applications, Int. J. Appl. Ceram. Technol. (2022) 2053–2063, https://doi.org/10.1111/ijac.14013, no. January.

[59] W. Choi, H. Shin, J.M. Kim, J. Choi, W. Yoon, Modeling and applications of electrochemical impedance spectroscopy (EIS) for Lithium-ion Batteries, J. Electrochem. Sci. Technol. 11 (2019) 1–8, https://doi.org/10.33961/jecst.2019.00528.

[60] R. Ravanamma, K.M. R, V.K. K, N. Ravi, Materials Today : proceedings Structure and morphology of yttrium doped barium titanate ceramics for multi-layer capacitor applications, Mater. Today Proc. 46 (1) (2021) 259–262, https://doi.org/10.1016/j.matpr.2020.07.646.

[61] L. Kola, A. Bihari, M. Rath, M.S.R. Rao, P. Murugavel, Impedance characteristics and PTCR e ff ect in lead free BaTi 1- x Sn x O 3 piezoceramics, Mater. Res. Bull. 106 (June) (2018) 371–378, https://doi.org/10.1016/j.materresbull.2018.06.021.